Unusual glass-forming ability induced by changes in the local atomic structure in Ti-based bulk metallic glass

2007 J. Phys.: Condens. Matter 19 196104

(http://iopscience.iop.org/0953-8984/19/19/196104)

IOP PUBLISHING JOURNAL OF PHYSICS: CONDENSED MATTER

J. Phys.: Condens. Matter **19** (2007) 196104 (13pp) doi:10.1088/0953-8984/19/19/196104

Unusual glass-forming ability induced by changes in the local atomic structure in Ti-based bulk metallic glass

Y C Kim[1,5], H J Chang[2], D H Kim[2], W T Kim[3] and P R Cha[4]

[1] Division of Materials Science and Engineering, Korea Institute of Science and Technology, PO Box 131, Cheongryang, Seoul 130-650, Korea
[2] Center for Non-crystalline Materials, Department of Metallurgical Engineering, Yonsei University, Seoul 120-749, Korea
[3] Department of Physics, Chongju University, Chongju 360-764, Korea
[4] School of Advanced Materials Engineering, Kookmin University, 861-1, Chongnung-dong, Songbuk-gu, Seoul 136-702, Korea

E-mail: chany@kist.re.kr (Y C Kim)

Received 9 November 2006, in final form 21 March 2007
Published 20 April 2007
Online at stacks.iop.org/JPhysCM/19/196104

Abstract

The effect of partial replacement of Cu by Be in $Ti_{50}Cu_{32}Ni_{15}Sn_3$ alloy on the thermal properties, structure, and forming ability of an amorphous phase were investigated by differential scanning calorimetry (DSC), x-ray diffraction (XRD), extended x-ray absorption fine structure (EXAFS), and high-resolution transmission electron microscopy (HRTEM). $Ti_{50}Cu_{25}Ni_{15}Sn_3Be_7$ alloy shows enhanced glass-forming ability, enabling one to fabricate a fully amorphous bulk metallic glass sample 2 mm in diameter by injection casting. With the replacement, the supercooled liquid region ΔT_x ($= T_x - T_g$, where T_x is the crystallization temperature and T_g is the glass transition temperature) decreased from 73 to 45 K and the reduced glass transition temperature T_{rg} ($= T_g/T_l$, where T_l is the liquidus temperature) increased from 0.53 to 0.57. The amorphous $Ti_{50}Cu_{25}Ni_{15}Sn_3Be_7$ phase showed a formation of short-range-ordered clusters 1–2 nm in size, which is attributed to the strong interaction between Ti and Be. The results show that ΔT_x can be used as a thermal parameter reflecting the glass-forming ability of the alloy only when the phase formed during crystallization is the same as the phase competing with the glass transition during solidification.

(Some figures in this article are in colour only in the electronic version)

[5] Author to whom any correspondence should be addressed.

1. Introduction

It has been known that the amorphous structure of bulk metallic glasses in some alloys contains quenched-in nuclei or short-range order (SRO) clusters [1–5], which may be related to the atomic configuration in the highly undercooled liquid state. Since most bulk metallic glasses are multi-component systems consisting of more than three elements, the atomic configuration is complex, and it is an important parameter affecting the thermal and physical properties [6–9]. In most bulk metallic glass system, an ideal random distribution of constituting elements is not expected to take place especially in a highly undercooled liquid state due to strong attractive interactions between the elements. As the undercooling increases, the tendency to form preferred atomic pairs or SRO clusters increases due to a reduced entropy contribution at lower temperature. The evolution of SRO clusters in amorphous alloys is affected by the alloy composition and cooling rate [10–12].

The presence of SRO clusters in an undercooled liquid state may give either a positive or negative effect in enhancing the glass-forming ability (GFA), depending on the role of the clusters in the nucleation of the crystalline phase. For a glass transition, the nucleation and growth of a competing crystalline phase should be suppressed during solidification. If the SRO clusters in an undercooled liquid do not act as nucleating sites for the crystalline phase, the GFA of the alloy is expected to be high, due to increased viscosity. It has been reported that the icosahedral short-range order or medium-range order (MRO) in the Zr-based amorphous alloys reduces the nucleation kinetics of crystalline phase and increases the glass-forming ability [12, 13]. If the SRO clusters promote the nucleation of a crystalline phase, which is the competing phase with the glass transition during solidification, the presence of SRO clusters deteriorates the GFA. However, the crystalline phase formed with help from the clusters is different from the competing phase, the formation of SRO clusters in an undercooled liquid can improve the GFA.

The range of the supercooled liquid region ($\Delta T_x = T_x - T_g$ where T_x is the crystallization temperature and T_g is the glass transition temperature), is known as one of thermal parameters reflecting the GFA of an alloy [14, 15]. The value of ΔT_x represents the degree of stability of the undercooled liquid against crystallization. As the value of ΔT_x increases, the stability of the undercooled liquid increases. Many alloys having ΔT_x larger than 100 K show high GFA [6–8]. However, there are many exceptions reported. Alloy systems with small ΔT_x (less than 60 K) often show a GFA as high as an alloy having large ΔT_x. Even though ΔT_x in the Cu–Ti–Zr–Ni–Si system is ∼45 K, a fully amorphous bulk specimen 6 mm in diameter can be manufactured by the injection-casting technique [16].

In this study, the effect of partial replacement of Cu by Be in $Ti_{50}Cu_{32}Ni_{15}Sn_3$ alloy on the glass-forming ability has been investigated by using thermal analysis, x-ray diffraction, extended x-ray absorption fine structure, and high-resolution transmission electron microscopy to establish the effect of SRO clusters on the glass-forming ability and crystallization behaviour.

2. Experimental procedures

The $Ti_{50}Cu_{32}Ni_{15}Sn_3$ and $Ti_{50}Cu_{25}Ni_{15}Sn_3Be_7$ alloys were prepared by arc melting high-purity Ti(99.99%), Cu(99.99%), Ni(99.99%), Sn(99.99%) and Cu–4 wt% Be master alloy under an Ar atmosphere. Rapidly solidified ribbon (∼30 μm thick) and bulk specimens were prepared by melt spinning and injection casting, respectively. High-resolution transmission electron microscopy (HRTEM) and x-ray diffraction (XRD; Rigaku, RINT 2200) with Cu Kα radiation source ($\lambda = 1.5405$ Å) experiments were performed to study the structure of the ribbons. Differential scanning calorimetry (DSC; Perkin Elmer DSC7) was carried out to determine

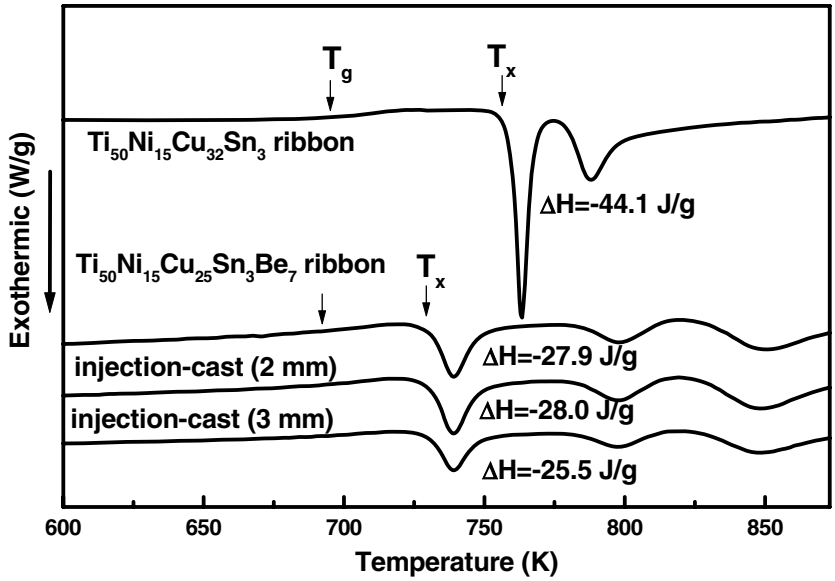

Figure 1. DSC traces obtained from melt-spun $Ti_{50}Cu_{32}Ni_{15}Sn_3$ and $Ti_{50}Cu_{25}Ni_{15}Sn_3Be_7$, and injection-cast $Ti_{50}Cu_{25}Ni_{15}Sn_3Be_7$ amorphous alloys.

the glass transition temperature (T_g), and crystallization temperature (T_x) of specimens. XRD experiments were used routinely to identify the crystalline phase present in the sample. To analyse the local atomic structure, transmission extended x-ray absorption fine structure (EXAFS) was carried out at room temperature at station BL3C1 of the Pohang Light Source (PLS). Absorption spectra were recorded at Cu (8.979 keV), Ni (8.333 keV) and Ti (4.966 keV) K edges. Samples were prepared as ribbons with thickness of 5–10 μm after grinding. A Si(111) double-crystal monochromator was used with detuning to 70% in intensity to eliminate high-order harmonics. The x-ray intensity was monitored with a nitrogen-gas filled ionization chamber detector. The EXAFS oscillations, $k \times \chi^3(k)$, were extracted using Autobk code and then Fourier transformed over the k range of 2–12.8 Å^{-1}. The EXAFS data were analysed by the conventional procedure described elsewhere [17, 18].

3. Results

3.1. Enhanced glass-forming ability

Figure 1 shows the DSC curves obtained during continuous heating of the as-melt-spun and injection-cast $Ti_{50}Cu_{25}Ni_{15}Sn_3Be_7$ samples. For comparison, the DSC curve from the as-melt-spun $Ti_{50}Cu_{32}Ni_{15}Sn_3$ sample is also included. The $Ti_{50}Cu_{32}Ni_{15}Sn_3$ alloy exhibited two exothermic reactions during crystallization, while the $Ti_{50}Cu_{25}Ni_{15}Sn_3Be_7$ alloys exhibited three exothermic reactions. The glass transition temperatures remained almost the same for the two alloys. However, the crystallization temperature, defined by the onset temperature of the first exothermic peak, decreased from 759 to 733 K, resulting in a decrease in ΔT_x from 73 to 45 K, with the addition of Be. The DSC trace from the injection-cast $Ti_{50}Cu_{32}Ni_{15}Sn_3Be_7$ sample with diameter of 2 mm is almost identical to that from the melt-spun ribbon, indicating that a fully amorphous structure was formed during solidification. However, the specimen with diameter of 3 mm showed slightly smaller exothermic heat for crystallization than the melt-

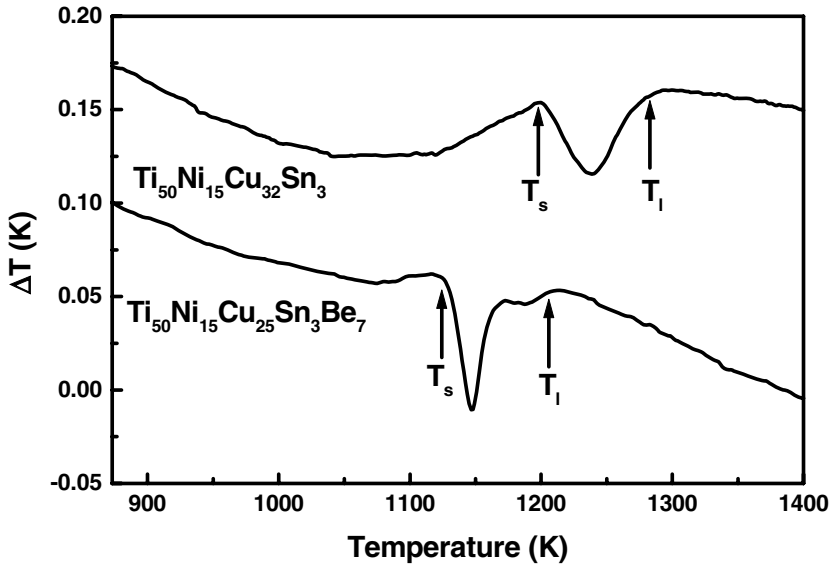

Figure 2. DTA traces obtained from melt-spun $Ti_{50}Cu_{32}Ni_{15}Sn_3$ and $Ti_{50}Cu_{25}Ni_{15}Sn_3Be_7$ amorphous alloys.

spun ribbon specimen, indicating that a partial crystallization takes place during solidification to form a mixture of crystalline and amorphous phases. Similar injection casting experiments were performed for $Ti_{50}Cu_{32}Ni_{15}Sn_3$ alloy to estimate the GFA. Even the alloy sample of 1 mm diameter showed a mixture of amorphous and crystalline phases, clearly indicating that the partial substitution of Cu by Be improved the GFA.

Figure 2 shows the DTA curves obtained during continuous heating of the as-melt-spun $Ti_{50}Cu_{32}Ni_{15}Sn_3$ and $Ti_{50}Cu_{25}Ni_{15}Sn_3Be_7$ samples. The onset and end temperatures of the melting endotherm (T_s and T_l) were 1205 and 1283 K, respectively, for the $Ti_{50}Cu_{32}Ni_{15}Sn_3$ alloy, and 1122 and 1207 K for the Be-containing alloy. A significant decrease in melting temperature was obtained by the partial replacement of Cu by Be in the $Ti_{50}Cu_{32}Ni_{15}Sn_3$ alloy. The reduced glass transition temperatures ($T_{rg} = T_g/T_l$) were 0.53 and 0.57 for the $Ti_{50}Cu_{32}Ni_{15}Sn_3$ and $Ti_{50}Cu_{25}Ni_{15}Sn_3Be_7$ alloys, respectively. ΔT_x and T_{rg} have been used for reflecting the GFA. From our results, T_{rg} exhibits good correlation with the GFA, while ΔT_x does not. Details regarding the poor correlation of ΔT_x are discussed below.

3.2. Crystallization behaviour

As shown in figure 1, the amorphous $Ti_{50}Cu_{32}Ni_{15}Sn_3$ and $Ti_{50}Cu_{25}Ni_{15}Sn_3Be_7$ phases, respectively, crystallized through two-step and three-step exothermic reactions. In order to identify each exothermic reaction, heat treatments were performed to complete each exothermic reaction. Figure 3(a) shows x-ray diffraction patterns obtained from the melt-spun specimens after the first and second exothermic reactions for the $Ti_{50}Cu_{32}Ni_{15}Sn_3$ alloy. For comparison, the x-ray diffraction pattern from the as-melt-spun specimen is also included. The amorphous $Ti_{50}Ni_{15}Cu_{32}Sn_3$ alloy crystallized through a precipitation of cubic TiNi and Ti_2Ni phases in the first crystallization step, followed by transformation into a mixture of Ti(Ni, Cu), TiCu, Ti_3Sn phases at higher temperature. Figure 3(b) shows x-ray diffraction patterns obtained from the melt-spun specimens after the first, second and third exothermic reactions for the $Ti_{50}Cu_{25}Ni_{15}Sn_3Be_7$ alloy. For comparison, the x-ray diffraction pattern from the as-melt-

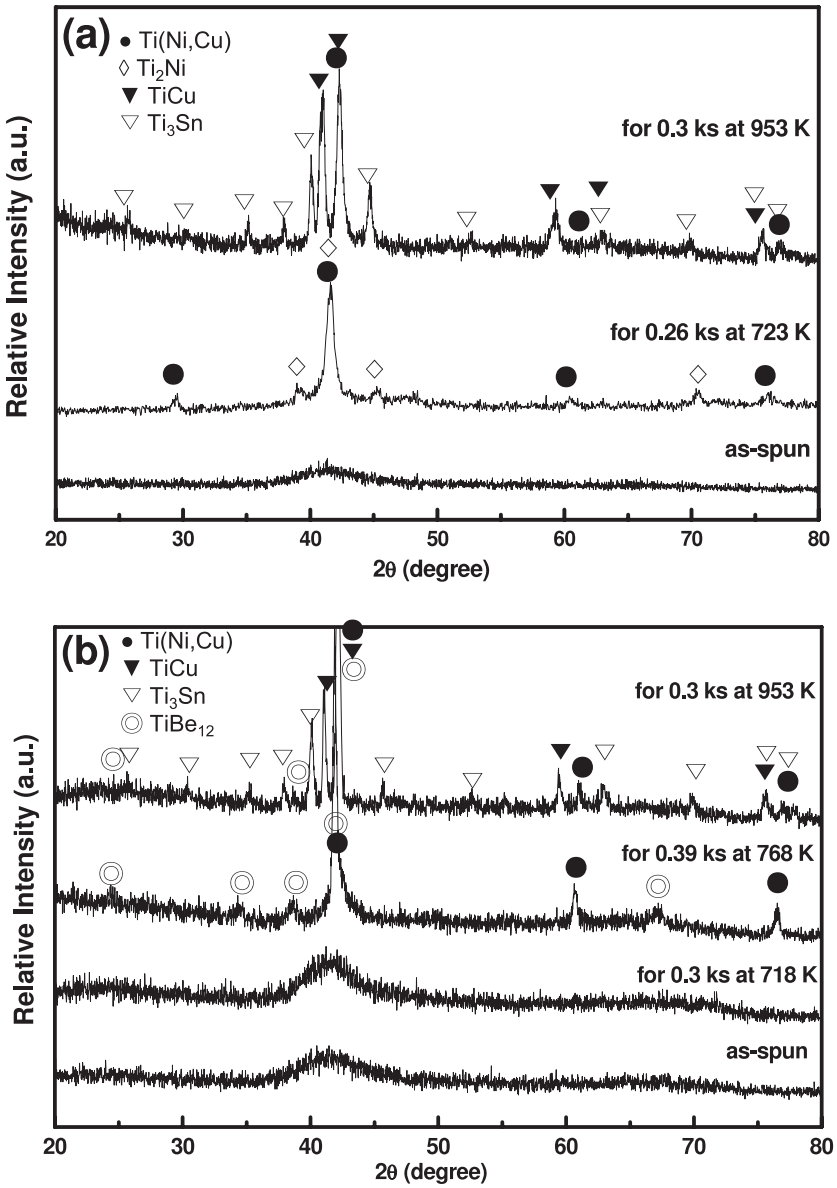

Figure 3. X-ray diffraction patterns obtained from: (a) $Ti_{50}Ni_{15}Cu_{32}Sn_3$; and (b) $Ti_{50}Ni_{15}Cu_{25}Sn_3Be_7$ ribbons in the as-spun state and after isothermal heat treatments.

spun specimen is also included. Even after the first exothermic reaction, a broad diffraction peak appeared without sharp crystalline peaks, indicating the precipitation of a nanoscaled crystalline phase. The specimen annealed to complete the second exothermic reaction showed a mixture of cubic TiNi and $TiBe_{12}$ phases. After the third exothermic reaction several crystalline phases appeared [19].

Figure 4(a) shows an HRTEM image obtained from $Ti_{50}Cu_{25}Ni_{15}Sn_3Be_7$ ribbon specimens after the first exothermic reaction. The HRTEM image showed fine crystalline particles with a diameter of about 5 nm surrounded by the residual amorphous phase. Several diffraction

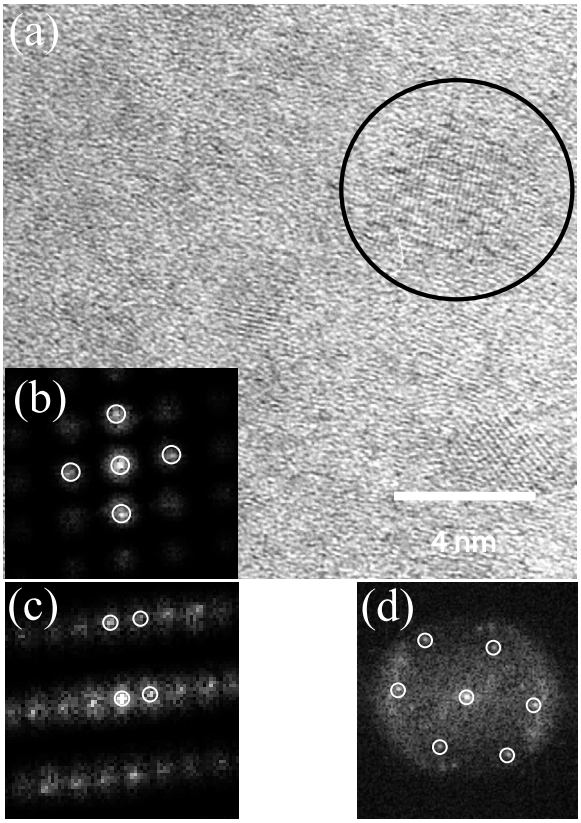

Figure 4. (a) HRTEM image obtained from $Ti_{50}Cu_{25}Ni_{15}Sn_3Be_7$ ribbon specimens heat treated up to 758 K, just the end temperature of the first crystallization reaction and (b) the simulation pattern obtained from the circled region by fast Fourier transforms.

patterns were obtained by Fourier transformation of the lattice fringes in the HRTEM images as shown in figures 4(b)–(d). Unfortunately, none of the diffraction patterns corresponded to any crystalline phases reported in the Ti–Ni–Cu–Sn(–Be) system. The observation of nanoscaled crystalline particles was in agreement with the corresponding XRD pattern in figure 3(b), consisting of a broad diffraction peak without clear crystalline peaks. The high density of the nanoscaled crystalline phase seems to be related to the SRO clusters in the as-melt-spun amorphous phase, which will be shown later.

Figure 5(a) shows an HRTEM image obtained from a $Ti_{50}Cu_{25}Ni_{15}Sn_3Be_7$ ribbon specimen heated up to 790 K, i.e. the initial stage of the second crystallization reaction. The HRTEM image showed a clear lattice image, corresponding to a crystalline particle with a diameter of about 10 nm surrounded by the residual amorphous phase. As shown in figure 5(b), the diffraction pattern obtained by Fourier transforms of the lattice fringes is in accord with the [111] zone of the cubic TiNi structure. The formation of TiNi phase in the second exothermic reaction is in agreement with the XRD result shown in figure 3(b).

4. Discussion

Partial replacement of Cu by Be changes the thermal properties of the $Ti_{50}Cu_{32}Ni_{15}Sn_3$ alloys. The $Ti_{50}Cu_{25}Ni_{15}Sn_3Be_7$ alloy shows a significantly lower melting temperature (by about 75 K)

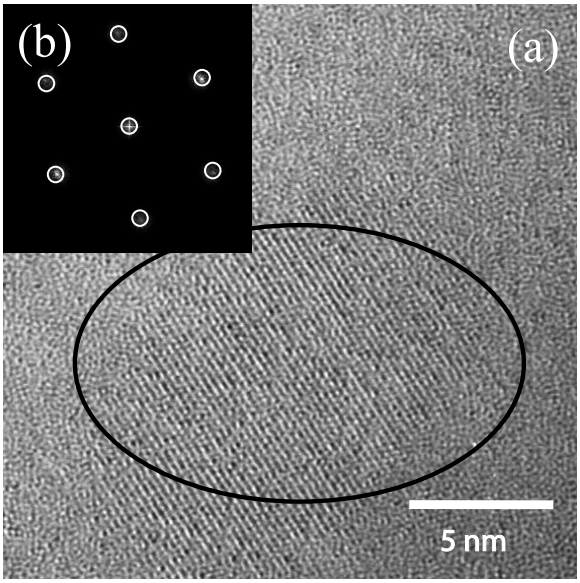

Figure 5. (a) HRTEM image obtained from a $Ti_{50}Cu_{25}Ni_{15}Sn_3Be_7$ ribbon specimen heat treated up to 780 K, just before the second crystallization reaction and (b) the simulation pattern obtained from the circled region by fast Fourier transforms.

than the $Ti_{50}Cu_{32}Ni_{15}Sn_3$ alloy (figure 2), indicating that the partial replacement stabilized the liquid phase with respect to the crystalline phase. The glass transition temperature of the amorphous phases is insensitive to the replacement but the crystallization onset temperature decreases from 759 K for the amorphous $Ti_{50}Cu_{32}Ni_{15}Sn_3$ phase to 733 K for the amorphous $Ti_{50}Cu_{25}Ni_{15}Sn_3Be_7$ phase. With the replacement, the supercooled liquid region ΔT_x decreases from 73 to 45 K and the reduced glass transition temperature T_{rg} increases from 0.53 to 0.57. The $Ti_{50}Cu_{25}Ni_{15}Sn_3Be_7$ alloy shows enhanced GFA, enabling one to fabricate a fully amorphous bulk metallic glass sample 2 mm in diameter by injection casting. The enhanced GFA with decrease of ΔT_x, which reflects the thermal stability, may be related to the change of local atomic structure.

Figures 6(a) and (b) show HRTEM images obtained from the as-melt-spun $Ti_{50}Cu_{32}Ni_{15}Sn_3$ and $Ti_{50}Cu_{25}Ni_{15}Sn_3Be_7$ alloys. In comparison with the $Ti_{50}Cu_{32}Ni_{15}Sn_3$ alloy ribbon (figure 6(a)), the HRTEM image from the $Ti_{50}Cu_{25}Ni_{15}Sn_3Be_7$ alloy ribbon shows some features suggesting the presence of local ordering (marked by the circles in figure 6(b)). The marked regions with size of 1–2 nm can be classified as SRO or MRO clusters, and hereafter they will be referred to as SRO clusters. Their volume fraction is estimated to be about 2% from the HRTEM observation. Figure 6(c) shows an HRTEM image obtained from the injection-cast $Ti_{50}Cu_{25}Ni_{15}Sn_3Be_7$ alloy rod with diameter 2 mm. The same type of clusters as in the as-melt-spun ribbon was observed, and the fraction of SRO clusters was also almost the same as that of the as-melt-spun ribbon, indicating that the formation of SRO clusters in the amorphous $Ti_{50}Cu_{25}Ni_{15}Sn_3Be_7$ alloy is not strongly related to the cooling rate. Unfortunately, it was difficult to identify the clusters due to the small size and difficulty in microchemical analysis of Be.

The presence of SRO clusters in an undercooled liquid state may give either a positive or negative effect in enhancing the GFA, depending on the role of the clusters in the nucleation of the crystalline phase. For a glass transition, the nucleation and growth of a competing

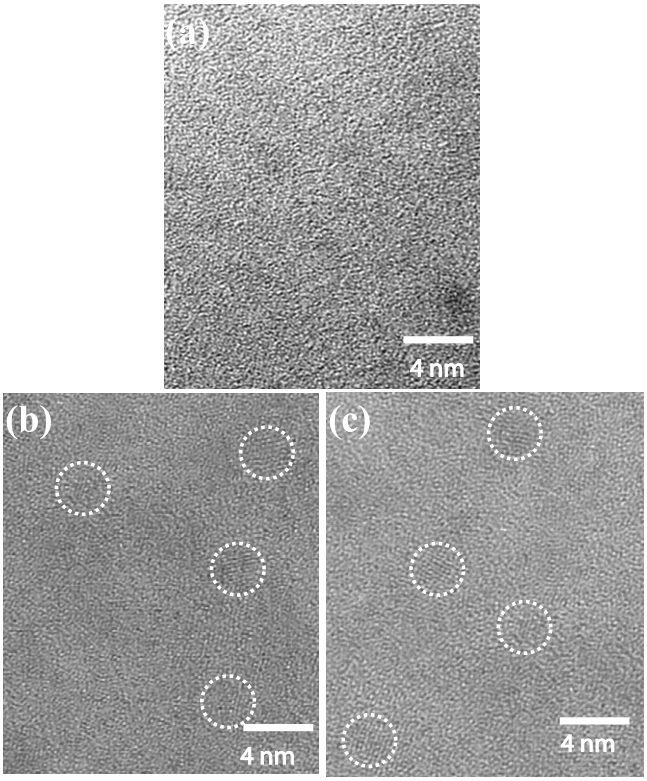

Figure 6. HRTEM images of the rapidly quenched ribbon for (a) the amorphous $Ti_{50}Cu_{32}Ni_{15}Sn_3$, (b) $Ti_{50}Cu_{25}Ni_{15}Sn_3Be_7$ alloys and (c) as-cast specimen for the $Ti_{50}Cu_{25}Ni_{15}Sn_3Be_7$ alloys.

crystalline phase should be suppressed during solidification. If the SRO clusters in an undercooled liquid do not act as nucleating sites for the crystalline phase, the GFA of the alloy is expected to be high due to reduced nucleation kinetics, as in the Zr-based amorphous alloys [12, 13]. If the SRO clusters promote the nucleation and growth of a crystalline phase, which is the competing phase with the glass transition during solidification, the presence of SRO clusters will deteriorate the GFA. It has been reported that the density of icosahedral clusters in $Al_{80}Ni_{20}$ alloy melt is very high [20], but the GFA is low because an icosahedral phase forms easily from the clusters during solidification. However, when the crystalline phase formed from the clusters is different from the competing phase, the formation of SRO clusters in an undercooled liquid may improve the GFA.

It is important to know which crystalline phase is competing with the glass transition during solidification because the nucleation and growth of the crystalline phase should be suppressed to form a fully amorphous specimen. To identify the competing crystalline phase in the $Ti_{50}Cu_{25}Ni_{15}Sn_3Be_7$ alloy solidification, x-ray diffraction experiments were performed on bulk specimens. Figure 7 shows the x-ray diffraction results obtained from the injection specimens with diameters of 2 and 3 mm. While the XRD pattern for the specimen with diameter of 2 mm showed a broad halo pattern without any sharp crystalline peaks, the XRD pattern for the specimen with diameter of 3 mm consisted of sharp crystalline peaks superimposed on the diffuse halo pattern of the glassy phase. As shown in figure 1, the specimen with diameter of 2 mm solidified into a fully amorphous structure. But the specimen

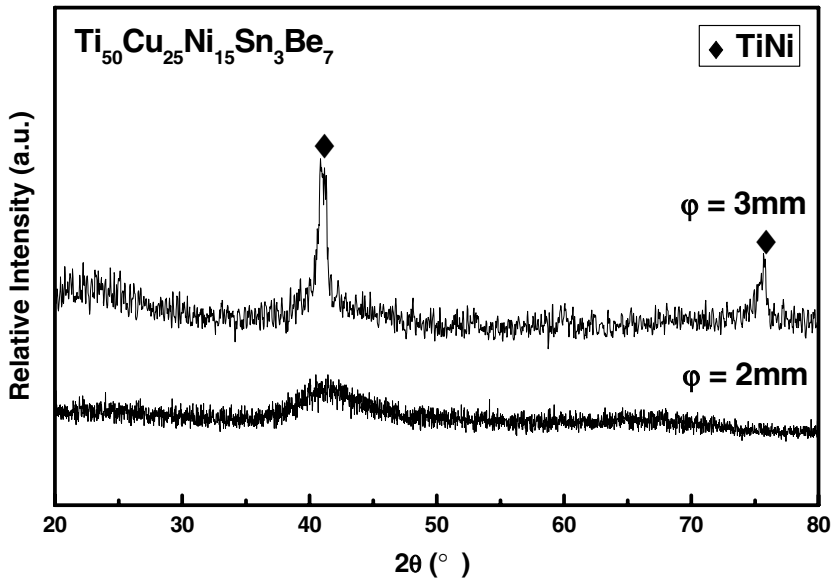

Figure 7. Typical XRD traces obtained from injection-cast $Ti_{50}Ni_{15}Cu_{25}Sn_3Be_7$ alloy rods with 2 mm and 3 mm diameter, respectively.

with diameter of 3 mm was solidified into a mixture of crystalline and amorphous phases. The crystalline peaks could be identified to a cubic TiNi phase with lattice constant of $a = 3.09$ Å. Therefore, it can be concluded that the cubic TiNi phase is formed first from the liquid during solidification if the cooling rate is not enough high to form a glass transition. To form a fully amorphous specimen, the nucleation and growth of the cubic TiNi phase should be suppressed. It was also found that the same crystalline phase is competing with the glass transition during the solidification of $Ti_{50}Cu_{32}Ni_{15}Sn_3$ alloy.

In order to investigate the effect of Be on the GFA and crystallization behaviour in more detail, the local atomic structures have been analysed using EXAFS. Figures 8(a)–(c) show the results of inverse Fourier transformation, FT$[k \times \chi^3(k)]$, for Ti, Cu and Ni K edges, respectively, (without phase shift correction) obtained from the melt-spun amorphous $Ti_{50}Cu_{32}Ni_{15}Sn_3$ and $Ti_{50}Cu_{25}Ni_{15}Sn_3Be_7$ alloys. In the case of the Ti-edge spectrum (figure 8(a)), three main peaks with peak positions at 1.63, 1.99 and 2.42 Å, corresponding to Ti–O, Ti–(Ni, Cu) and Ti–Ti bonding, respectively, were observed. From the analysis of XANES (x-ray absorption near-edge structure) data (not shown), it has been concluded that the amount of O in the sample is not so large as to affect the intrinsic electronic structure of metal Ti. Therefore, the peak from Ti–O bonding will not be considered any more. The reason for the reduced amplitude with addition of Be is not clear, but it may be due to the scavenging effect of Be. With addition of Be the amplitude of the second peak decreased without peak shift. On the other hand, the amplitude of the third peak from Ti–Ti bonding remained almost the same, but the peak position shifted to a smaller r value (2.42 $\rightarrow$ 2.33 Å). In the case of the Cu- and Ni-edge spectra (figures 8(b) and (c)), peaks from each bonding were superimposed; therefore only one broad main peak was observed. It can be noticed that the amplitude of the peaks in the Ti-edge spectrum is significantly low when compared with that in the Cu- and Ni-edge spectra, implying more enhanced disordering around Ti atoms. The EXAFS results indicate that, with addition of Be, the amount of Ti–(Cu, Ni) bonding decreased, implying that the formation of

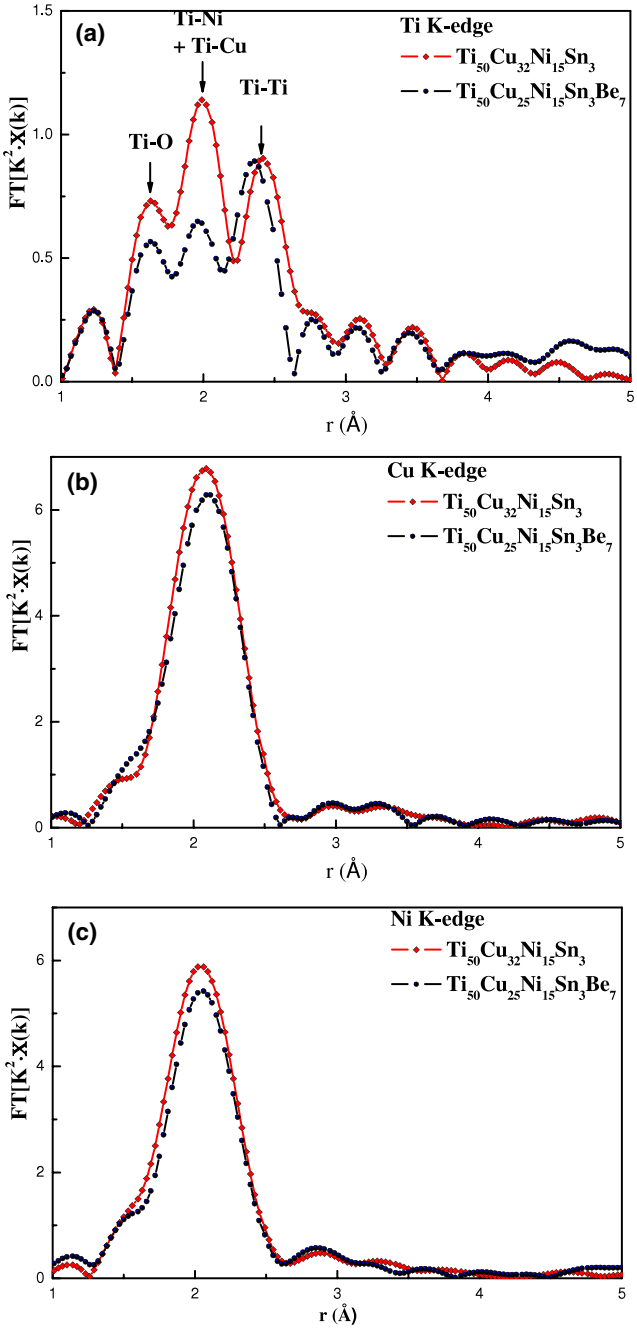

Figure 8. The inverse Fourier transformation, FT[$k \times \chi^3(k)$], obtained from (a) Ti, (b) Cu and (c) Ni K edges in a restricted imaginary r range (1–5 Å).

TiNi can be prevented. The formation of fine nanocrystals (not TiNi) during the early stage of crystallization (figure 4) supports the amount of Ti–(Cu, Ni) bonding being significantly less with addition of Be, preventing the formation of TiNi phase directly from the amorphous phase.

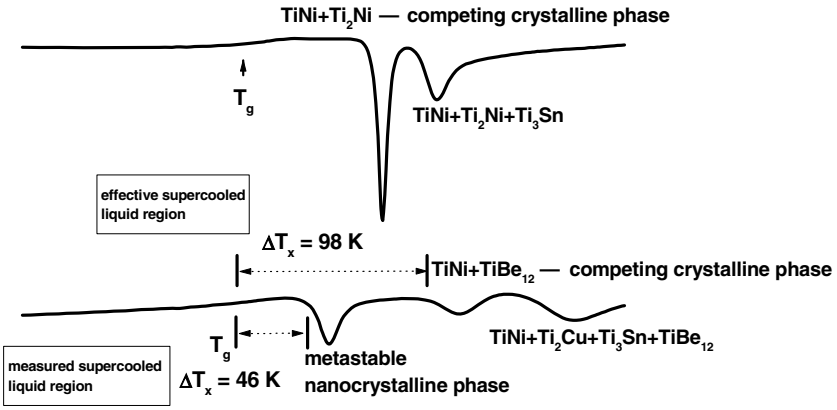

Figure 9. Schematic description of effective supercooled liquid region in the DSC curve for an alloy forming a metastable nanocrystal phase as well as competing crystalline phase.

The Ti-edge spectrum also indicates that the Ti–Be bond with Be addition may have an effect on the decrease of r value of the Ti–Ti bond.

As mentioned previously, the cubic TiNi phase is competing with the glass transition during solidification of the $Ti_{50}Cu_{32}Ni_{15}Sn_3$ and $Ti_{50}Cu_{25}Ni_{15}Sn_3Be_7$ alloys. During heating of the amorphous $Ti_{50}Cu_{32}Ni_{15}Sn_3$ alloy, the TiNi phase forms in the first exothermic reaction with an onset temperature of 759 K. But the partial replacement of Cu by Be changes the crystallization kinetics, which is related to the change in atomic structure described previously. During heating of the amorphous $Ti_{50}Cu_{25}Ni_{15}Sn_3Be_7$ phases, nanoscaled unidentified crystalline particles form first before the formation of the TiNi phase at higher temperature. The SRO clusters seems to be responsible for the decreases in crystallization onset temperature as shown in figure 1. The present results indicate that the SRO cluster is not directly related to the formation of the TiNi phase, which is competing with the glass transition, but contributes to the formation of the nanocrystalline phase in the first exothermic reaction. As a result, T_x decreases, resulting in a smaller ΔT_x, as shown in figure 1. The crystallization reaction for the competing crystalline phase (TiNi) is not the first exotherm but the second exotherm, as illustrated in a schematic DSC curve shown in figure 9.

The formation of a metastable phase prior to the thermodynamically stable phase can be explained by *Ostwald's step rule*, which means that crystallization from a solution occurs in steps in such a way that often thermodynamically unstable phases occur first, followed by the thermodynamically stable step. Consider a liquid material whose stable crystalline phase has face-centred cubic (FCC) structure. With mild undercooling, its crystalline phase always nucleates due to the small kinetic energy barrier to the crystalline phase and large atomic mobility. With large undercooling, however, the kinetic energy barrier become too large (the atomic mobility become too small) to nucleate the stable crystalline phase and another metastable or unstable phase with smaller kinetic energy barrier can form first. This is the case when the body-centred cubic (BCC) phase first nucleates in a melt with FCC stable crystalline phase with severe undercooling [21]. The formation of a metastable phase observed in our experiment is also the same case. As the first peak in DSC curve for the alloy containing Be is located at a lower temperature than for the alloy without Be, and at this temperature Ti and Ni does not have enough atomic mobility, the metastable phase observed in the alloy with Be at the first peak is not formed by the diffusion and combination of Ti and Ni. Hence, we propose another scenario for the first peak at lower temperature and more diffusive peaks. Passing

T_g, the diffusion of the smallest species, Be, becomes much more activated than other larger elements; this was already observed in [22]. The metastable (or unstable) phase containing Be is likely to have the smallest kinetic energy barrier and to be formed prior to the stable TiNi or $TiBe_{12}$. Indeed, the metastable phase looks very distorted, and shows a structure close to the disordered mother phase, which also suggests that the kinetic energy barrier from the amorphous mother phase to the metastable one can be smaller than that to the crystalline stable phase. The existing metastable phases retard the nucleation and growth of the competing crystalline phase (TiNi) because they expend Ti or other elements in the matrix and reduce the driving force to the competing crystalline phase.

Considering the crystallization of the competing crystalline phase, the effective supercooled liquid region representing the GFA can be as large as 98 K for the Be-containing alloy, which can explain the enhancement of the GFA. The values of the reduced glass transition temperature, 0.53 and 0.57 for the amorphous $Ti_{50}Cu_{32}Ni_{15}Sn_3$ and $Ti_{50}Cu_{25}Ni_{15}Sn_3Be_7$ alloys, respectively, matches well with the improvement of the GFA with the addition of Be in Ti–Ni–Cu–Sn alloy. The present results indicate that the supercooled liquid region ΔT_x can be used as a thermal parameter reflecting the GFA of the alloy only when the crystallization phase is the same as the phase competing with the glass transition during solidification. In this case the effective supercooled liquid region, which is defined as the temperature difference between T_g and the onset temperature of the exotherm corresponding to the formation of the competing phase, may be a thermal parameter reflecting the GFA of the alloy. This may be the reason why the co-relationship between ΔT_x and GFA is rather poor in many alloy systems [23].

5. Conclusions

Partial replacement of Cu by Be changed the thermal properties of the $Ti_{50}Cu_{32}Ni_{15}Sn_3$ alloys. $Ti_{50}Cu_{25}Ni_{15}Sn_3Be_7$ alloy shows enhanced GFA, enabling one to fabricate a fully amorphous bulk metallic glass sample 2 mm in diameter by injection casting. With the replacement, ΔT_x decreased from 73 to 45 K and the reduced glass transition temperature T_{rg} increased from 0.53 to 0.57. The amorphous $Ti_{50}Cu_{25}Ni_{15}Sn_3Be_7$ phase showed the formation of SRO clusters 1–2 nm in size, which is attributed to the strong interaction between Ti and Be. The supercooled liquid region ΔT_x can be used as a thermal parameter reflecting the GFA of the alloy only when the crystallization phase is the same as the phase competing with the glass transition during solidification.

Acknowledgments

This research was supported by a grant (code#:06K1501-00410) from ‘Center for Nanostructured Materials Technology’ under ‘21st Century Frontier R&D Programs’ of the Korean Ministry of Science and Technology, and the Korea Institute of Science and Technology. DHK wishes to express appreciation for the partial financial support provided by the Creative Research Initiatives of the Korean Ministry of Science and Technology and the Basic Research Program (R01-2006-000-10891-0) of Korea Science and Engineering Foundation, Republic of Korea. PRC also wishes to express appreciation for the partial financial support provided by the SRC/ERC program of MOST/KOSEF (R11-2005-048-0000-0). We are grateful to the authorities concerned with the Pohang Light Source (PLS) for XAS measurements, especially Nak Eon Sung and Dr Min Kyu Kim with whom we had fruitful discussion.

References

[1] Herlach D M 1994 *Mater. Sci. Eng.* R **12** 177
[2] Ohkubo T, Kai H, Makino A and Hirotsu Y 2001 *Mater. Sci. Eng.* A **312** 274
[3] Holland-Moritz D, Herlach D M and Urban K 1993 *Phys. Rev. Lett.* **71** 1196

[4] Imafuku M, Yaoita K, Sato S, Zhang W, Inoue A and Waseda Y 2001 *Mater. Sci. Eng.* A **304–306** 660
[5] Schumacher H, Herr U, Oelgeschlaeger D, Traverse A and Samwer K 1997 *J. Appl. Phys.* **82** 155
[6] Peker A and Johnson W L 1993 *Appl. Phys. Lett.* **63** 2342
[7] Park E S, Kang H G, Kim W T and Kim D H 2002 *J. Non-Cryst. Solids* **298** 15
[8] Sung D S, Kwon O J, Fleury E, Kim K B, Lee J C, Kim D H and Kim Y C 2004 *Met. Mater. Int.* **10** 575
[9] Kim W B, Ye B J and Yi S 2004 *Met. Mater. Int.* **10** 1
[10] Xing L Q, Eckert J, Loser W and Schultz L 1998 *Appl. Phys. Lett.* **73** 2110
[11] Lee J K, Bae D H, Kim W T and Kim D H 2004 *Mater. Sci. Eng.* A **375–377** 332
[12] Xing L Q, Hufnagel T C, Eckert J, Löser W and Schultz L 2000 *Appl. Phys. Lett.* **77** 1970
[13] Mattern N, Kühn U, Hermann H, Ehrenberg H, Neuefeind J and Eckert J 2002 *Acta Mater.* **50** 305
[14] Inoue A, Zhang T and Masumoto T 1993 *J. Non-Cryst. Solids* **156–158** 473
[15] Li Y, Jones H and Davies H A 1992 *Scr. Metall. Mater.* **26** 1371
[16] Park E S, Lim H K, Kim W T and Kim D H 2002 *J. Non-Cryst. Solids* **298** 15
[17] Rehr J J, Leon J M, Zabinsky S I and Albers R C 1991 *J. Am. Chem. Soc.* **113** 5135
[18] O'Day P A, Rehr J J, Zabinsky S I and Brown G E 1994 *J. Am. Chem. Soc.* **116** 2938
[19] Kim Y C, Kim W T and Kim D H 2002 *Mater. Trans. JIM* **43** 1243
[20] Dubois J M, Montoya F and Back C 1994 *Mater. Sci. Eng.* A **178** 285
[21] Ishihara K N, Maeda M and Shingu P H 1985 *Acta Metall.* **33** 2113
[22] Tang X P, Geyer U, Busch R, Johnson W L and Wu Y 1999 *Nature* **402** 160
[23] Waniuk T A, Schroers J and Johnson W L 2001 *Appl. Phys. Lett.* **78** 1213